A Novel Framework for Enhancing Resilience of Urban Underground Drainage Networks in IoT Sponge City

Hongyan Dui, Ran Li, Huanqi Zhang, Shaomin Wu

***Abstract*—Amid increasing extreme rainfall events, urban pluvial flooding poses a significant threat to city infrastructure and public safety. To address the limitations such as poor coordination between subsystems and low resilience of conventional IoT frameworks in underground drainage networks, this paper proposes a resilience-driven architecture termed R⁴-UDN. The framework integrates four signature mechanisms: event-triggered sensing, resimulation-in-loop, cascade-aware control, and cross-layer KPI alignment, forming a closed-loop management system. The paper introduces a multi-stage resilience index and embeds it into a semi-Markov cascade model to capture system performance dynamically. Furthermore, it optimizes the resilience and sequence-sensitive cost. A case from Chengdu, China, is studied to confirm that the proposed method significantly enhances resilience compared to conventional strategies, validating the practical value of R⁴-UDN for enhancing the resilience of sponge city underground drainage systems.**

***Index Terms*—resilience optimization, urban drainage networks, IoT architecture, hydrodynamic simulation coupling, multi-objective optimization**

NOMENCLATURE

i	index of a node in the drainage network under study, $i = 1,2,\cdots,m$
j	index of a side of the drainage network under study, $j = 1,2,\cdots,n$
$C_{total,i}$	the total cost of the base repair costs of node i under study
$C_{total}(\mathcal{S})$	sequence-sensitive total cost of strategy $\mathcal{S}$
ε_{ij}	the failure propagation coefficient
$\mathcal{E}$	the set of sides of the drainage network
$E(t)$	the number of connected edges at time t
$F_i(t)$	the failure state function of node i
$\Pi(\Delta t)$	the node transition probability matrix of the urban underground drainage network
$H_i(t)$	the water level of node i
$\mathcal{N}$	the set of nodes of the drainage network
$N_{exceed}(t)$	the number of nodes in the network when the water level exceeds the design limit
P_d	the lowest multidimensional performance value from t_0 to t_r
$P(t)$	the multidimensional performance of the urban underground drainage network
$P_Q(t)$	the flow performance of node i
$P_H(t)$	the water level performance of node i
$P_D(t)$	the degree performance of node i
$Q_{i,in}$	the total inflow to node i from upstream links and external sources
$Q_{i,out}$	the total outflow from node i
$Q_i(t)$	the net nodal flow at node i
$Q'_j(\mathrm{t})$	the flow of node j after the failure of node i is repaired
R	comprehensive resilience index of the urban underground drainage network
R_{res}	resilience to maintain the performance in the face of an initial disturbance
R_{abs}	resilience to absorb impact of a disturbance during the performance degradation phase
R_{rec}	resilience to recover an initial or steady-state level after the multidimensional performance $P(t)$ drops to the lowest
$\mathcal{S}$	a strategy of candidate failure nodes' repair sequence
$S(t)$	the system state at time t, $S(t) \in \{S_0, S_1, S_2, S_3\}$
t_0	the moment of disruption
t_b	the moment when the multidimensional performance $P(t)$ becomes smaller than the standard threshold
t_d	the moment when the multidimensional performance $P(t)$ reaches the lowest value
t_e	the moment when the multidimensional performance $P(t)$ returns to the final steady state, or the completion time
t_r	the moment when the multidimensional performance $P(t)$ first exceeds the standard threshold
w_i	weights of each resilience indicator

This work was supported by the Natural Science Foundation of Henan Province (No. 252300421005). (Corresponding author: Hongyan Dui, Shaomin Wu).

Hongyan Dui, Ran Li, Huanqi Zhang are with School of Management, Zhengzhou University, Zhengzhou 450001, China (email: duihongyan@zzu.edu.cn; liran2022@stu.zzu.edu.cn; zzuzhq@gs.zzu.edu.cn).

Shaomin Wu is with the Kent Business School, University of Kent, Canterbury, CT2 7FS Kent, U.K. (e-mail: S.M.Wu@kent.ac.uk).

I. INTRODUCTION

Urban Underground Drainage Networks (UDN) are defined as critical urban infrastructure systems comprising interconnected nodes and pipe segments designed to manage stormwater and mitigate pluvial flooding. Recently, urban flooding has emerged as one of the most pressing challenges in modern cities, driven by rapid urbanization and increasingly frequent extreme rainfall events [1]. Underground drainage networks, as critical components of urban infrastructure, play a pivotal role in mitigating pluvial floods but may be highly vulnerable due to their concealed structures, aging pipelines, and limited adaptability [2], [3]. The concept of sponge cities has been widely promoted as a sustainable strategy to address these challenges, emphasizing infiltration, retention, storage, purification, and controlled drainage [4]. However, realizing these functions in underground drainage systems requires more intelligent, resilient, and adaptive mechanisms.

With the rise of smart city technologies, the Internet of Things (IoT) has been introduced to enhance monitoring and control of drainage systems. By integrating real-time sensing, communication, and data-driven optimization, IoT-enabled infrastructures can improve both responsiveness and stability [5], [6], [7]. A recent review paper underlines that IoT-enabled smart cities face persistent challenges of heterogeneity, scalability, and security, which constrain the resilience and adaptability of underground infrastructures [8]. IoT-based monitoring research has demonstrated that zone-differentiated, time-constrained flow capacity models utilizing mobile sensors can significantly enhance coverage efficiency and reliability in large-scale urban pipeline systems [9]. Recent research advances in the IoT architectures propose a physical–information–functional framework with multi-level closed loops, which overcomes the coarse granularity of traditional layered models and enhances scalability and resilience [10], [11]. Multi-objective optimization methods further support decision-making by balancing resilience, economic costs, and environmental impacts, as shown in studies on low-impact development [12], [13] and urban flood resilience [14], [15]. Large-scale multi-objective optimization approaches have been recognized as effective tools for managing conflicting goals in intelligent IoT systems, supporting adaptive decision-making across complex networked infrastructures [16]. In the broader reliability optimization field, selective maintenance studies demonstrate that machine learning–enhanced dynamic programming can address multi-stage decision problems under constrained resources [17], [18].

Multi-objective optimization techniques have been widely adopted to support complex decision-making in urban management contexts [19]. Among them, the Non-dominated Sorting Genetic Algorithm II (NSGA-II) has proven effective in identifying Pareto-optimal solutions for trade-offs between cost, resilience, and environmental performance [20], [21]. In parallel, the Storm Water Management Model (SWMM) has become a standard simulation tool for evaluating rainfall–runoff processes, drainage capacities, and control strategies in both short-term and long-term hydrological scenarios [22], [23]. Recent studies have increasingly combined NSGA-II and SWMM to optimize drainage network configurations and low-impact development schemes, integrating intelligent control and data-driven learning to enhance flood mitigation and real-time system adaptability [24], [25]. However, most of these applications remain static, lacking explicit modeling of system resilience or cascading dynamics under extreme rainfall. This gap underscores the need for a more integrated optimization framework that couples hydrodynamic simulation with real-time IoT feedback and multi-stage resilience assessment.

At the same time, resilience as a system property has evolved from a simple recovery capacity to multidimensional concepts encompassing resistance, absorption, and recovery phases [26]. Research on dynamic reliability assessment highlights that sensor degradation and imperfect multilevel data substantially reduce trustworthiness, underscoring the need for resilient IoT architectures that jointly update system and sensor states [27], [28]. Recent research further extended resilience research toward spatiotemporal performance modeling within IoT-enabled system-of-systems [29]. Studies on interdependent infrastructures have highlighted that preparedness-oriented strategies can significantly enhance multistate resilience, emphasizing the importance of proactive planning prior to disruptive events [30]. These advances have broadened the analytical and operational tools available for urban drainage management.

Nevertheless, several critical gaps remain. First, most IoT-based drainage studies employ the conventional four-layer architecture: the physical, perception, communication, and application layers, which are loosely coupled. Such designs rarely address cross-layer dependencies, especially in the context of cascading disruptions. Second, current optimization models often emphasize static or single-stage objectives, neglecting the temporal dynamics of resilience during extreme rainfall events. Advances in multisource information fusion demonstrate that conflicting and imprecise data can be effectively integrated through a two-stage optimization approach, providing methodological support for resilient underground drainage assessment [31]. Network-based resilience frameworks demonstrate that dynamic performance can be quantified through topology evolution and state transitions, offering tools to assess

cascading disruptions in infrastructure systems [32], [33]. Third, underground-specific challenges, such as signal attenuation in wells and the propagation of cascading failures across drainage nodes, are not adequately incorporated into the architecture or optimization frameworks [34]. Recent studies emphasize that IoT reliability must capture the coupled degradation of physical units and information networks, where cascading failures across layers critically affect overall system performance [35]. These gaps limit the ability of existing approaches to provide reliable and resilience-oriented decision support in real-world sponge city applications.

To address these limitations, this study proposes a resilience-driven IoT architecture, R⁴-UDN (Resilience-Ready, Risk-Aware, Resimulation-in-loop Redundant for Underground Drainage Networks). Unlike the standard four-layer model, R⁴-UDN introduces four key mechanisms: (i) event-triggered sensing associated with resilience thresholds, (ii) resimulation-in-loop multi-objective optimization, (iii) cascade-aware sensing–control coupling, and (iv) cross-layer KPI alignment. Based on this architecture, we develop a comprehensive framework that incorporates a multi-stage resilience index, a resimulation-in-loop semi-Markov cascade model, and a sequence-sensitive cost formulation.

The main contributions of this paper are fourfold:

- Architecture-level novelty: R⁴-UDN incorporates four resilience-driven mechanisms into a closed-loop architecture, surpassing the loose coupling typical of conventional IoT layers.
- Metric-level novelty: A multi-stage resilience index is created, with discretization aligned to SWMM hydrodynamic steps for reproducibility.
- Model-level novelty: A resimulation-in-loop semi-Markov cascade model is developed, incorporating estimation of state transitions and explicit inclusion of cascade propagation coefficients.
- Optimization-level novelty: A sequence-sensitive cost function is proposed to optimize the resilience, capturing both timing and order of interventions, and solved using NSGA-II to produce actionable Pareto solutions.

The remainder of this paper is organized as follows. Section II presents the research problem to be addressed and the R⁴-UDN architecture. Section III presents the multidimensional performance model of urban underground drainage network. Section IV presents the methodological framework for resilience assessment and optimization. Section V presents a case study in Chengdu, China, illustrating the effectiveness of the proposed approach under real-world conditions of extreme rainfall. Section VI allocates to our conclusion.

II. Problem Description and R⁴-UDN Architecture

R⁴-UDN is defined as a resilience-driven IoT architecture tailored for Urban Underground Drainage Networks (UDN), grounded in four core dimensions: Resilience-Ready, Risk-Aware, Resimulation-in-loop, and Redundant. The framework operates through four integrated mechanisms: event-triggered sensing for dynamic data acquisition, resimulation-in-loop for multi-objective optimization, cascade-aware control for optimized recovery sequencing, and cross-layer KPI alignment for unified system performance evaluation. The traditional sponge city planning emphasizes infiltration, storage, purification, and delayed discharge, aiming to restore urban water balance through green infrastructure. These methods have successfully reduced surface runoff and enhanced water quality. However, most implementations concentrate on surface facilities and lack mechanisms to address the complex interactions within underground drainage systems, where cascading failures and delayed recovery often impact a city's flood resilience. This highlights the need to incorporate intelligent monitoring, real-time control, and multi-objective optimization to expand sponge city principles from surface water management to underground infrastructure systems. Accordingly, we extend the surface peak-shaving logic of sponge-city practices downward to the real-time resilience regulation of underground cascade networks, and organize the subsequent performance definitions, triggering rules, and optimization models under the R⁴-UDN framework.

First, it is important to clarify the differences in the challenges faced by traditional sponge city technologies and underground drainage networks. Traditional sponge city practices mainly focus on surface processes through "infiltration–detention–storage–purification–discharge," aiming to reduce early rainfall peaks and pollution. However, during long-duration extreme rainfall and secondary blockages, the underground drainage system's performance becomes critical for preventing cascading flooding from point to area and for ensuring quick recovery. Surface LID facilities mainly influence infiltration and runoff. In contrast, the underground system is limited by in-pipe hydraulic capacity, nodal connectivity redundancy, and communication and control reachability, each with different time frames and control options. Therefore, this chapter emphasizes how the underground network responds, absorbs, and recovers under extreme conditions. It introduces a resilience-driven cross-layer closed-loop (R⁴-UDN) that integrates monitoring, communication, control, and optimization into an actionable strategy chain.

As a key component within the sponge city concept, Fig. 1 shows the operational process and interaction mechanism between the urban underground drainage system and the

urban river system, as well as the relationship among the external environment, the urban pipeline network, and the river network. It highlights the differences in drainage paths of the urban underground drainage system under normal and abnormal conditions. When rainfall or upstream water inflow occurs in the external environment, precipitation or surface runoff first enters the urban underground drainage system through catchment wells. It then flows into inspection wells via branch pipes and eventually collects at the drainage outlets through the main pipes.

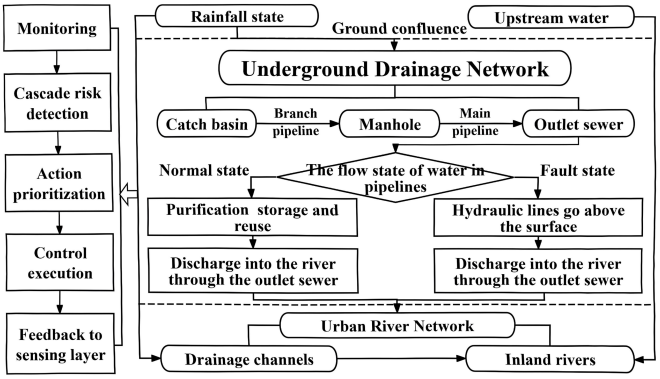

Fig. 1. Mechanisms of urban underground drainage networks.

Under normal conditions, stormwater collected within a nodal-pipe network is purified, temporarily stored, and carefully released into downstream river systems. However, during extreme rainfall, structural failures or hydraulic overloads can happen, causing flow congestion, water level rises, and surface ponding. If these problems are not properly managed, they can lead to widespread urban flooding. Emergency response protocols must be swiftly activated to lower systemic risk, such as rerouting excess water to nearby open channels or river outlets. Ultimately, the river network serves as the final stage in stormwater management, linking artificial drainage systems with the natural hydrological environment.

Urban underground drainage networks present inherent challenges for effective monitoring and adaptive control, due to their concealed layout, risks of cascading failure, and difficulties in maintaining reliable communication underground. The traditional IoT four-layer architecture typically includes the physical, perception, communication, and application layers. While it provides basic sensing and data transfer, it often lacks strong cross-layer integration, resilience mechanisms, and the capacity to handle extreme rainfall events. To address these issues, this study introduces a resilience-driven IoT architecture called R^4-UDN (Resilience-Ready, Risk-Aware, Resimulation-in-loop, Redundant for Underground Drainage Networks), which transitions from a static layered model to a dynamic, cross-layer, closed-loop system.

The R^4-UDN architecture features four key mechanisms that transform the architecture from a loose collection of layers into a resilience-focused framework designed to handle cascading disruptions and improve adaptive recovery. Fig. 2 illustrates the IoT architecture of the urban underground drainage network based on R^4-UDN.

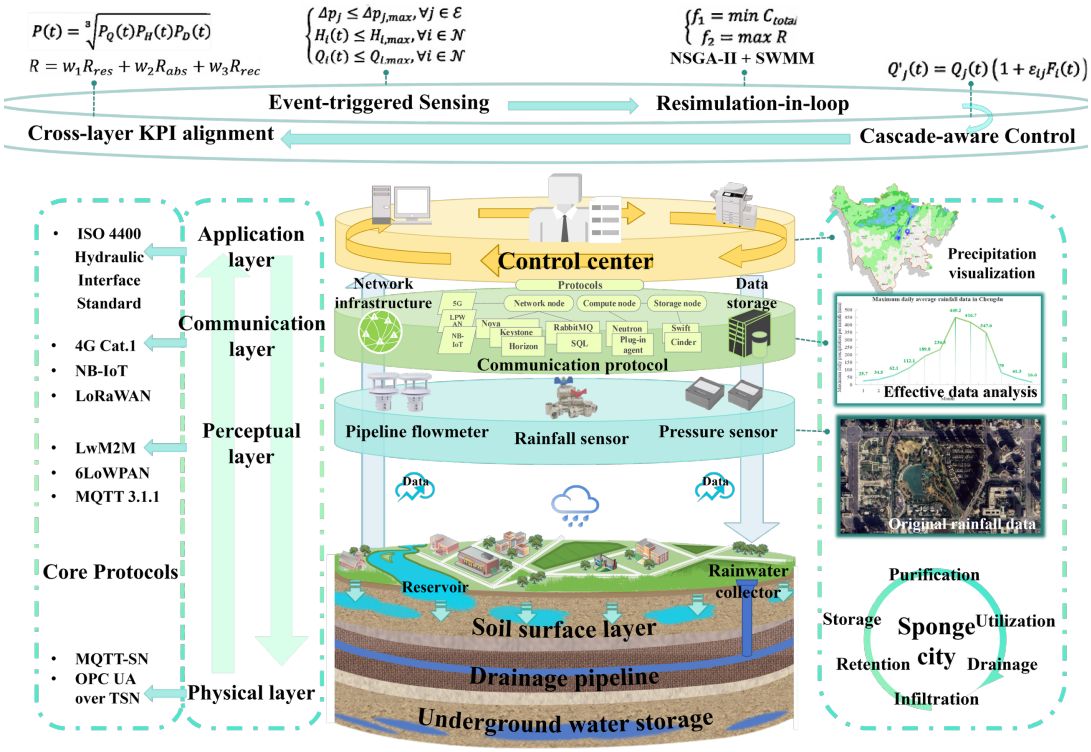

Fig. 2. An IoT architecture for underground drainage networks.

(1) Event-triggered sensing by resilience states.

Instead of continuous uniform monitoring, R⁴-UDN adopts an event-triggered scheme: when the multidimensional performance $P(t)$ falls below predefined thresholds, the system activates high-frequency data acquisition and deploys localized, dense sensing. This selective activation directly corresponds to resilience stages (resistance, absorption, recovery), reducing energy consumption while enhancing monitoring sensitivity under stress conditions.

(2) Resimulation-in-loop multi-objective optimization.

Instead of learning control policies via reinforcement learning, candidate intervention plans are generated by NSGA-II and evaluated by the SWMM hydraulic simulator. SWMM acts as the feasibility and performance oracle, rejecting hydraulically infeasible candidates and returning resilience- and risk-related metrics. Iterating this "optimize, restimulate score" loop yields a Pareto set that balances resilient gains against implementation and operating costs while remaining hydraulically valid under shock scenarios.

(3) Cascade-aware sensing–control coupling.

The propagation coefficients of cascading failures are directly integrated into prioritizing control and repair actions. When a node failure jeopardizes downstream structures, its cascade influence dictates the urgency of intervention. This forms a closed loop from cascade awareness to cascade-driven response, allowing the system to address not only local faults but also systemic risks.

(4) Cross-layer KPI alignment.

R⁴-UDN consolidates sensing reliability, data availability, hydraulic safety constraints, and system-level resilience outcomes (performance degradation and recovery profiles) into a unified KPI set used throughout Section III and Section IV. These KPIs are computed consistently from SWMM simulations and resilience evaluation, then fed into the NSGA-II objective and constraint design so that perception quality, hydraulic feasibility, resilience gain, and intervention cost are optimized jointly rather than assessed in isolation. This cross-layer alignment enables end-to-end, scenario-based decision-making beyond the traditional four-layer model's independent objectives.

In summary, R⁴-UDN introduces structural and mechanism innovations, incorporating event-triggered monitoring, multi-objective optimization and cascade-aware control into a unified, resilience-focused framework. These mechanisms collectively expand sponge city functions beyond traditional infiltration, retention, and drainage, adding a new capability—real-time resilience regulation of underground networks. The architecture thus lays the groundwork for subsequent multi-stage resilience modeling and NSGA-II-based optimization.

III. Multidimensional Performance Modeling

This study examines the operational behavior and fault response mechanisms of urban underground drainage networks under both normal and extreme conditions. The node network model is developed based on core principles of fluid dynamics and hydrology. First, it is assumed that the nodes and connections of the urban underground pipe network are linked and can create a complete flow pathway. Then, nodes represent different rainwater facilities, including catch basins, inspection wells, pumping stations, and outfalls. And sides represent the pipelines connecting nodes to nodes.

The selection of flow rate, water level, and nodal connectivity as key indicators for multidimensional performance assessment is grounded on both hydrodynamic theory and empirical relevance to system functionality. The flow rate directly reflects the system's drainage capacity and the effectiveness of hydraulic conveyance under various loading conditions [12]. Water level indicates the degree of system stress and the proximity to overflow or surcharge conditions, serving as a critical proxy for flood risk [22]. Nodal connectivity, often expressed as topological degree, captures the structural robustness of the drainage network and reflects the potential for alternative routing or redundancy in flow paths. These indicators represent physical, hydraulic, and structural dimensions of performance, providing a comprehensive basis for quantifying resilience in cascading failure scenarios. Their integration enables the model to assess not only whether the system is operational, but also how effectively it can resist, absorb, and recover from disruptions.

In this paper, hydraulic dynamics are represented by EPA SWMM's dynamic-wave scheme, which solves the Saint-Venant momentum on links coupled with nodal continuity, updating heads and discharges at each hydraulic step Δt under surcharge, storage, and component capacity constraints [36]. For each node i with spatial coordinate x ($x \geq 0$) and time t ($t \geq 0$), we explicitly define the flow rate $Q_i(x,t)$, wetted area $A_i(x,t)$, and hydraulic head $H_i(x,t)$ as functions of space and time. The node flow conservation equation is formulated as:

$$\frac{\partial Q_i(x,t)}{\partial t} + \frac{\partial}{\partial x}\left(\frac{Q_i^2(x,t)}{A_i(x,t)}\right) + gA_i(x,t)\frac{\partial H_i(x,t)}{\partial x} + gA_i(x,t)S_f = 0, \quad (1)$$

where $\frac{\partial Q_i(x,t)}{\partial t}$ is the local acceleration, $\frac{\partial}{\partial x}\left(\frac{Q_i^2(x,t)}{A_i(x,t)}\right)$ captures momentum transfer due to velocity gradients along the conduit, $gA_i(x,t)\frac{\partial H_i}{\partial x}(x,t)$ represents the driving force arising from water surface slope, while S_f is the frictional

resistance slope drop of the water flow, which is reflected in the form of the slope drop, and $gA_i(x,t)S_f$ corresponds to the resistance induced by boundary friction, commonly modeled by the Manning equation.

The focus of this paper is to improve the responsiveness of the urban underground drainage network under heavy rainfall and flooding. Therefore, for a fixed node i, we aggregate the nodal flow terms as:

$$\sum_{t=1}^{M} Q_i(t) = \sum_{t=1}^{M} Q_{i,in}(t) - \sum_{t=1}^{M} Q_{i,out}(t), \quad (2)$$

where t is the current simulation time ($t = 1, \dots, M$) indexes the SWMM hydraulic time steps and i ($i \in \mathcal{N}$) denotes a fixed node. $Q_i(t)$ is the net nodal flow at node i, and positive when net inflow increases the local storage, $Q_{i,in}(t)$ is the inflow to node i at time t from upstream links and external sources, $Q_{i,out}(t)$ is the outflow from node i at time t. The summation aggregates the time series at node i only.

The pressure drops at both ends of a pipe can be expressed as:

$$\Delta p_j(t) = k l_j Q_j^2(t), \quad (3)$$

where $\Delta p_j(t)$ is the pressure drops in the drainage network of side j, k is the pressure loss coefficient, and l_j is the length of the side j. From this, the constraints of the urban underground drainage network can be expressed as:

$$\begin{cases} \Delta p_j \le \Delta p_{j,max}, \forall j \in \mathcal{E} \\ H_i(t) \le H_{i,max}, \forall i \in \mathcal{N} \\ Q_i(t) \le Q_{i,max}, \forall i \in \mathcal{N} \end{cases}, \quad (4)$$

where $H_i(t)$ is the water level of node i, $\Delta p_{j,max}$ is the maximum admissible pressure drop across side j, $H_{i,max}$ is the maximum allowable hydraulic head at node i, and $Q_{i,max}$ is the maximum allowable discharge at node i. These limits represent design/operational capacities used to prevent surcharge and structural risk, and are taken from SWMM parameters or field specifications.

To unify water-level and flow exceedance in a single indicator for node-state discretization, we define the water-level exceedance ratio and the flow exceedance ratio as:

$$\rho_i^H(t) = \frac{H_i(t)}{H_{i,max}}, \quad (5)$$

and

$$\rho_i^Q(t) = \frac{Q_i(t)}{Q_{i,max}}. \quad (6)$$

The unified nodal exceedance ratio is then defined as $\rho_i(t) = \max\{\rho_i^H(t), \rho_i^Q(t)\}$. When $\rho_i(t) > 1$, at least one hydraulic capacity limit is exceeded at node i, indicating an abnormal condition that may trigger cascading effects on hydraulically connected neighbors.

Through the above analysis of node flow, water level, and topology with edges in the pipe network and the construction of the node flow model, this paper defines the value of the multidimensional performance of the urban underground drainage network at any time t as:

$$P(t) = \sqrt[3]{P_Q(t) P_H(t) P_D(t)}. \quad (7)$$

The multidimensional performance values, $P_Q(t)$, $P_H(t)$, and $P_D(t)$, in three dimensions of flow, water level, and degree at different moments are combined. Among them, the node flow performance $P_Q(t)$ is shown as:

$$P_{Q,i}(t) = \begin{cases} 1, & Q_i(t) \le Q_{max,i} \\ \dfrac{Q_{max,i}}{Q_i(t)}, & Q_i(t) > Q_{max,i} \end{cases}, \quad (8)$$

and

$$P_Q(t) = \frac{1}{N} \sum_{i=1}^{N} P_{Q,i}(t), \quad (9)$$

where $P_{Q,i}(t)$ is the flow performance of node i, N is the total number of nodes in the network.

The node water level performance $P_H(t)$ is computed by counting nodes whose water level does not exceed the allowable head, i.e., nodes satisfying $\rho_i^H(t) \le 1$, and divided by the total number of nodes:

$$P_H(t) = \frac{N - N_{exceed}(t)}{N}, \quad (10)$$

where $N_{exceed}(t)$ is the number of nodes in the network when the water level exceeds the design limit, N is the total number of nodes in the network.

The degree performance $P_D(t)$ of a node is defined as the ratio of the actual number of connected edges $E(t)$ of the node at the moment t to the initial number of connected edges E_0, which indicates the contribution of the number of edges connected by the node to the multidimensional performance of the urban underground drainage network:

$$P_D(t) = \frac{E(t)}{E_0}, \quad (11)$$

where E_0 is the number of connected edges at time $t = t_0$, that is, $E_0 = E(t_0)$. The more connected edges a node has, the more stable the network topology and the higher degree performance.

The above formulations establish a simplified but tractable representation of hydraulic and structural performance within the drainage network. Nevertheless, such abstractions cannot fully capture nonlinear processes such as dynamic wave propagation, surcharge pressure interactions, and coupled surface–subsurface flows. To ensure physical realism, the SWMM is employed in subsequent analyses as a hydrodynamic calibration tool. Detailed node and pipe attributes are imported into SWMM, and their simulation outputs are compared with theoretical performance indicators, thereby aligning the resilience assessment with both computational efficiency and hydraulic accuracy.

The system-level state is defined as a derived label from the multidimensional system performance $P(t)$. Specifically, we define $S(t) \in \{S_0, S_1, S_2, S_3\}$ by partitioning $P(t)$ into four intervals: S_0 corresponds to normal drainage (high performance), S_1 to mild waterlogging, S_2 to moderate flooding, and S_3 to severe flooding. Notably, $S(t)$ is a system

state label for resilience segmentation and result presentation, rather than a node state.

See Table I for a summary of the system-level state definition $S(t)$ based on $P(t)$.

TABLE I
DIFFERENT STATES OF URBAN UNDERGROUND DRAINAGE NETWORKS

System State	Description	Performance Range
Normal operation (S_0)	Stable discharge capacity and no observed degradation	$P(t) \geq 0.9$
Mild-damage (S_1)	Slight flow reduction: system maintains most functions	$0.7 \leq P(t) < 0.9$
Moderate failure (S_2)	Functionality is significantly impaired; partial blockage or reduced conveyance	$0.4 \leq P(t) < 0.7$
Severe failure (S_3)	Widespread hydraulic overload; multiple node failures	$P(t) < 0.4$

On this basis, the hydraulic–topological indicators obtained from the simplified model and SWMM simulations provide a basis for defining node-level state evolution under disturbance scenarios. For each node, node i for example, we define a four-level discrete state variable $X_i(t) \in \{X_0, X_1, X_2, X_3\}$, which serves as the state space in the semi-Markov process. The node state is determined by the unified nodal exceedance ratio $\rho_i(t)$ computed from SWMM outputs of nodal hydraulic head and discharge, as defined above.

TABLE II
NODE-STATE DEFINITION BASED ON UNIFIED NODAL EXCEEDANCE RATIO

Note State	$X_i(t) =$	Unified Nodal Exceedance Ratio
Normal	$X_i(t) = X_0$	$\rho_i(t) \leq 1$
Mild-damage	$X_i(t) = X_1$	$1 < \rho_i(t) \leq 1 + \delta_1$
Moderate failure	$X_i(t) = X_2$	$1 + \delta_1 < \rho_i(t) \leq 1 + \delta_2$
Severe failure	$X_i(t) = X_3$	$\rho_i(t) > 1 + \delta_2$

The threshold parameters δ_1 and δ_2 are determined empirically from SWMM simulations. Specifically, we collect the samples of all nodes and all hydraulic time steps under the simulated disturbance scenarios and set $1 + \delta_1$ and $1 + \delta_2$ to the 70th and 90th percentile values of the sampled with $\rho_i(t) > 1$, respectively. This data-driven calibration yields consistent state boundaries for discretizing node conditions into $X_i(t)$ and improves reproducibility.

Based on the calibrated state boundaries, the continuous surcharge ratio $\rho_i(t)$ is mapped to the discrete state sequence $X_i(t)$. To capture the temporal evolution of these states in the case study considered in this paper, we analyze the sojourn time (i.e., the duration a node remains in a specific state) across all simulated scenarios. Statistical analysis of the SWMM-derived trajectories indicates that, in this setting, the sojourn times are well characterized by a Weibull distribution, suggesting non-exponential residence behavior and thus departures from pure Markovian transitions with evident "delay" effects. Consequently, we employ the Weibull distribution to fit these durations, with the shape parameter k and scale parameter λ estimated directly from the simulated data.

We denote the one-step transition matrix of the node state $X_i(t)$ by $\Pi(\Delta t)$. Time is discretized by the SWMM hydraulic step Δt. Cross-level transitions and recoveries are allowed. For example, at the time of failure, depending on the level of disaster impact, the node state may shift rapidly from X_0 to X_1 or X_2, or even directly to X_3 in extreme cases; with the repair of the failure and the recovery of the node, the state may gradually shift from X_3 to X_2, X_1 and finally back to X_0.

The one-step transition matrix is defined as:

$$\Pi(\triangle t) = [p_{m,n}], \tag{12}$$

where $p_{m,n}$ denotes the one-step transition probability from state X_m to X_n over the SWMM time step $\triangle t$. It can be expressed as:

$$p_{m,n} = \Pr\{X_{t+\triangle t} = n | X_t = m\}, m, n \in \{X_0, X_1, X_2, X_3\}, \tag{13}$$

with nonnegative entries and row sums equal to one:

$$\sum_{n=0}^{3} p_{m,n} = 1, p_{m,n} \geq 0. \tag{14}$$

These probabilities are estimated from simulation trajectories, historical records, and expert elicitation. In this paper, $\Pi(\Delta t)$ is estimated from SWMM–control trajectories by frequency counts.

Under this semi-Markovian framework, the state of a node is determined by $\rho_i(t)$, while the transition timing is governed by the Weibull distribution. This relationship is formalized through a semi-Markov kernel matrix $K(t) = [K_{m,n}(t)]$, where each element is defined as:

$$K_{m,n}(t) = p_{m,n} G_{m,n}(t), \tag{15}$$

where $p_{m,n}$ represents the one-step transition probability from state m to state n, and $G_{m,n}(t)$ denotes the cumulative distribution function (CDF).

Based on the above definitions, we construct a cascade failure propagation model to describe chain reactions triggered by node failures. For cascade modeling, we introduce a binary failure indicator $F_i(t) \in \{0,1\}$, where $F_i(t) = 1$ denotes that node i is in a failure condition. In the subsequent analysis, periods with degraded multidimensional performance below 0.9, corresponding to the system state $S(t) \in \{S_0, S_1, S_2, S_3\}$, are used to identify representative disturbance scenarios, while the cascade propagation itself is governed by $\{F_i(t)\}$. The binary failure indicator is defined as:

$$F_i(t) = \begin{cases} 1, & X_i(t) \in \mathcal{X}_{fail} \\ 0, & X_i(t) \notin \mathcal{X}_{fail} \end{cases}, \tag{16}$$

where $\mathcal{X}_{fail} = \{X_2, X_3\}$ denotes the set of failed states (failure and severe failure) in the node-level semi-Markov state space.

When node i enters a failed state, the disrupted drainage capacity may impose additional hydraulic load on neighboring or strongly connected nodes, which can trigger cascading failures across the network.

In practice, the SWMM-generated hydrodynamic time series (nodal heads, discharges, and surcharge conditions) are used to compute $\rho_i^H(t)$, $\rho_i^Q(t)$, and $\rho_i(t)$, ensuring that node states $X_i(t)$ are discretized from SWMM simulation outputs via the unified exceedance ratio $\rho_i(t)$, and the cascade failure indicator $F_i(t)$ is then obtained by mapping $X_i(t)$ to the failed-state set $\mathcal{X}_{fail}$.

The propagation process of cascade failure can be expressed as:

$$Q'_j(t) = Q_j(t)\left(1 + \varepsilon_{ij}F_i(t)\right), \tag{17}$$

where $Q'_j(t)$ represents the flow of node j after the failure of node i occurs (i.e., when $F_i(t) = 1$), $Q_j(t)$ is the original flow at node j, and ε_{ij} is the failure propagation coefficient.

To make ε_{ij} physically identifiable under the dynamically induced cascading mechanis, we quantify ε_{ij} as the normalized increase in the peak nodal exceedance caused by the failure of node i. Let t_f denote the failure triggering time such that $F_i(t_f) = 1$. Over a short transient window $[t_f, t_f + T]$, define the baseline and post-failure peak exceedance ratios of node j as:

$$\rho_j^{max} = \max_{t\in[t_f,t_f+T]} \rho_j(t), \tag{18}$$

and

$$\rho_{j|i}^{max} = \max_{t\in[t_f,t_f+T]} \rho_{j|i}(t), \tag{19}$$

where $\rho_j(t) = \max\{\rho_j^H(t), \rho_j^Q(t)\}$ and $\rho_{j|i}^{max}$ is computed under the contingency that node i has failed. The failure propagation coefficient is then evaluated by:

$$\varepsilon_{ij} = \frac{\left(\rho_{j|i}^{max} - \rho_j^{max}\right)_+}{\left(\rho_j(t_f) - 1\right)_+}, \qquad (x)_+ = \max(x, 0), \tag{20}$$

where $\rho_i(t_f) \neq 1$ so that the normalization is well-defined. This definition implies that ε_{ij} increases with the extent to which the failure of node i amplifies the transient overload tendency of node j.

The description of the cascade failure propagation mechanism in this section clarifies the linkage relationship between the failure states of the nodes. It provides basic theoretical support for the formulation of subsequent optimization strategies.

IV. Multi-stage Resilience Enhancement

We assume that the initial multidimensional performance of the urban drainage system is P_0, the moment of disruption is t_0, and the moment when the multidimensional performance $P(t)$ first exceeds the standard threshold is t_r. The lowest multidimensional performance from t_0 to t_r is P_d. The moment when the multidimensional performance $P(t)$ returns to the final steady state, or the completion time, is t_e.

a) Resistance Resilience

Resistance resilience quantifies the system's ability to maintain functional performance in the face of an initial disturbance. In this paper, the degree of performance degradation is calculated as:

$$R_{res} = \frac{P_d}{P_0}, \tag{21}$$

where P_d is the lowest multidimensional performance value from t_0 to t_r, P_0 is the initial multidimensional performance. The closer R_{res} is to 1, the stronger the urban underground drainage network's ability to resist external disturbances.

b) Absorption resilience

Absorption resilience measures the ability of urban subsurface drainage systems to absorb the energy or impact of a disturbance during the performance degradation phase, defined by the following equation:

$$R_{abs} = \frac{\int_{t_0}^{t_d} P(t)dt - P_d(t_d - t_0)}{(t_d - t_0)(b - P_d)}, \qquad t_d \neq t_0 \tag{22}$$

where $P(t)$ is the multidimensional performance of the underground drainage network, P_d is the lowest multidimensional performance value from t_0 to t_r, t_d is the moment when the multidimensional performance of the urban underground drainage network reaches the lowest point, and b is the baseline of performance optimization.

When the multidimensional performance of the urban underground drainage network drops below the baseline, the primary resilience of the system shifts to absorption resilience. The larger the value of absorption resilience, the stronger the urban underground drainage network's ability to absorb disturbance during the period of falling to its lowest point after the disturbance occurs.

c) Recovery Resilience

Recovery resilience measures the ability of an urban subsurface drainage system to recover to an initial or steady-state level after a performance nadir. Recovery resilience is defined as:

$$R_{rec} = \frac{\int_{t_d}^{t_r} P(t)dt - P_d(t_r - t_d)}{(t_r - t_d)(b - P_d)}, \qquad t_r \neq t_d \tag{23}$$

where t_r is the moment when the multidimensional performance $P(t)$ first exceeds the standard threshold, t_d is the moment when the multidimensional performance reaches the lowest point. The larger the value of recovery resilience, the stronger the recovery ability of the network.

The resistance resilience index is used to assess the ability of the urban underground drainage network to maintain its normal drainage state in the face of external impacts. The absorption resilience index reflects the potential of the urban underground drainage network to rebound to its normal drainage state after experiencing effects that lead to a decline

in performance. The recovery resilience index measures the ability of the urban underground drainage network to regain its high-performance state after failure.

The changes in the multidimensional performance and resilience indicators of urban underground drainage networks at different stages, without human intervention, are shown in Fig. 3.

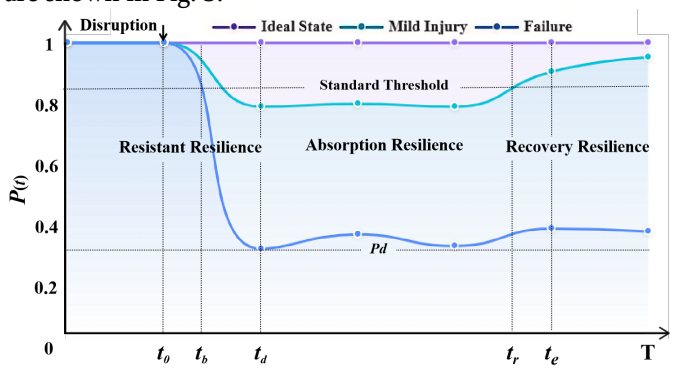

Fig. 3. Multidimensional performance evolution of urban underground drainage networks without human intervention.

In Fig. 3, all three scenarios represent the evolution of multidimensional performance in urban underground drainage networks under extreme rainfall conditions without human intervention or maintenance, thereby reflecting the system's natural degradation response in the absence of external recovery measures. The shaded areas represent the integral areas between the performance curve $P(t)$ and the minimum performance baseline in the absorption and recovery phases.

In practice, the performance curves $P(t)$ and stage-specific resilience indicators are derived from hydrodynamic time series generated by SWMM simulations. Outputs such as nodal water depth, pipe discharge, and surcharge conditions provide the empirical basis for quantifying resistance, absorption, and recovery. By grounding the theoretical definitions in physically based hydraulic responses, this coupling ensures that the resilience assessment remains both accurate and practically relevant, thereby providing reliable inputs for calculating the comprehensive resilience index.

The weighted summation of the resilience at different stages leads to a comprehensive resilience index of the urban underground drainage network R:

$$R = w_1 R_{res} + w_2 R_{abs} + w_3 R_{rec}. \quad (24)$$

Among them, w_1, w_2, and w_3 are the corresponding weights of each resilience indicator. In the baseline evaluation, equal weights are used to avoid subjective preference.

Based on the above definition of the multidimensional performance of the urban underground drainage network can well quantify the multi-stage resilience assessment in the face of extreme rainstorm impacts and provide a basic theoretical foundation and measurement tool for the subsequent optimization of the resilience of the urban underground drainage network under consideration of the cascading failure mechanism of the pipe network nodes.

Based on the resilience indicators, a multi-objective optimization model is established by considering the costs of each stage and comprehensively evaluating the long-term operation economy of the urban underground drainage network and the comprehensive ability to maintain the function under the simultaneous resistance to sudden shocks and continuous disturbances:

$$\begin{cases} f_1 = \min C_{total} \\ f_2 = \max R \end{cases}. \quad (25)$$

Among them, C_{total} includes the construction cost of the urban underground drainage network, the operation and maintenance cost, and the cost of repairing and replacing failed components of the urban underground drainage network, with the specific costs depending on the conditions of the particular target system. R is the comprehensive resilience index of the urban underground drainage network proposed in the above study.

In this study, the NSGA-II is used to solve the problem, and the specific steps of the algorithm implementation are as follows:

(1) Population initialization: the initial population consists of randomly generated candidate repair sequences (the decision variable) for the existing network under limited resources. The pipe layout and facility capacities are fixed system descriptors and are passed to SWMM as input parameters to evaluate the hydraulic feasibility and performance of each candidate sequence.

(2) Fitness assessment: calculating the fitness of everyone, i.e., the total cost of the urban subsurface drainage system versus the combined resilience value.

(3) Undominated sorting: the population is divided into different undominated fronts based on the fitness of individuals, where other individuals do not dominate the first undominated frontier individuals.

(4) Crowding degree computation: The crowding degree distance is computed for everyone in the nondominated frontier to ensure diversity in the solution set.

(5) Selection, crossover, and mutation: A tournament selection method was used to select superior individuals based on non-dominance rank and crowding, and crossover and mutation were performed to produce offspring individuals.

(6) Population update: The newly generated offspring are merged with the parent generation for non-dominated sorting and crowding calculation, and the top-ranked individuals are retained to form the next-generation population.

(7) Algorithm termination: the computation stops when the maximum number of iterations or convergence conditions are reached, and the Pareto-optimal solution set is output.

Fig. 4 illustrates the main flow of the NSGA-II employed in this study.

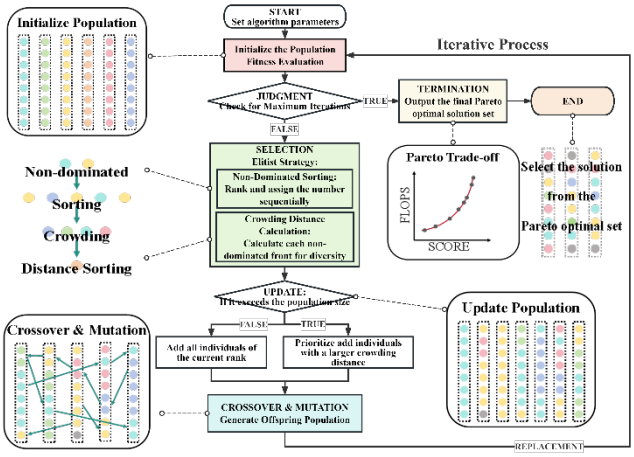

Fig. 4. Flowchart of the NSGA-II framework.

V. Case Study

Wuhou District, located in the central part of Chengdu, China, was selected as the study area (Fig. 5a). As a typical high-density urban zone characterized by mixed residential and commercial land use, Wuhou faces frequent pluvial flooding risks, particularly during the summer monsoon season.

A. Data Collection

According to the China Meteorological Administration, Chengdu experienced an average of 101.8 rainy days annually between 2013 and 2023, with peak hourly rainfall intensities often exceeding 100 mm/h. During the storm event on July 11–12, 2023, the district recorded a maximum rainfall intensity of 120 mm/h, resulting in widespread surface inundation and drainage overflow.

The physical characteristics of Wuhou's drainage system further exacerbate its vulnerability. Most pipelines were constructed before 2000 and are characterized by undersized diameters ($< 0.3\ m$), flat gradients, and sparse inspection wells—features commonly found in aging infrastructure across second-tier Chinese cities. Combined with limited sensor coverage and real-time monitoring, these conditions make the district a representative and challenging testbed for resilience assessment.

To ensure model realism, node and pipe data were obtained from the Chengdu Urban Construction Archives and the China Meteorological Data Center (http://data.cma.cn). The simulated drainage basin covers an area of 80.3 hectares and includes 83 nodes, 85 pipelines, and several inflow–outflow structures. Chengdu's growing population, which exceeded 21 million by 2023, further intensifies pressure on urban infrastructure.

Rainfall-runoff processes and flood propagation from the July 2023 storm were modeled using SWMM 5.2.1.0. Key inputs—such as node elevation, pipe slope, and diameter (Fig. 5b and Fig. 5c)—were extracted from geospatial datasets provided by the GSCloud platform (https://www.gscloud.cn). In the absence of complete real-time monitoring data, the model adopted calibrated parameter sets from similar catchments in Chengdu and referenced historical performance data to ensure simulation reliability and practical applicability.

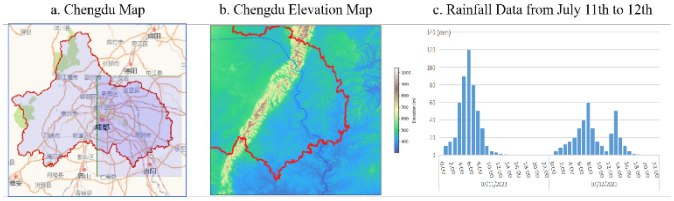

Fig. 5. Schematic diagram of geographic information extraction in Chengdu.

The simulation procedure adopted in this study is outlined below:

- Step 1: System Initialization: The state space, transition probabilities, cost structure, and performance parameters of the urban underground drainage network are defined.
- Step 2: Cascading Failure Simulation: The MCMC algorithm is employed to simulate state transitions and the propagation of cascading failures under heavy rainfall scenarios.
- Step 3: (Mechanism 4) Performance Evaluation via Cross-layer KPI Alignment: Based on the simulated state transitions, SWMM simulations are executed to generate raw hydrodynamic data, such as nodal water levels and flow rates. Crucially, strictly following the Cross-layer KPI alignment mechanism, these physical outputs are dynamically mapped to the unified multidimensional performance curve and the multi-stage resilience index. This process transforms discrete hydraulic data into holistic resilience metrics, providing the necessary quantitative basis for the subsequent optimization loop.
- Step 4: (Mechanism 2) Resimulation-in-loop Optimization: Instead of static assessment, the NSGA-II is coupled with SWMM in a closed loop. At each iteration, the 'resimulation-in-loop' mechanism triggers a hydrodynamic simulation to validate the hydraulic feasibility of candidate repair sequences, ensuring that the optimized strategy is not just mathematically optimal but physically valid.
- Step 5: Result Analysis: The Pareto-optimal solutions are analyzed to assess the effectiveness of the optimized

repair strategy in enhancing system-wide resilience.

B. SWMM Model Calibration and Validation

The EPA SWMM 5.2.1.0 used in this paper is an open-source urban stormwater management model developed by the U.S. Environmental Protection Agency (EPA). It is capable of comprehensively simulating urban rainfall runoff, pipe water transport, and sponge facility operation effects, making it suitable for accurate hydrological and hydraulic analysis. Meanwhile, SWMM can be efficiently coupled with optimization algorithms, such as NSGA-II, to achieve rapid data interaction and iterative optimization through programming.

During the construction of the SWMM simulation platform, node and pipe data for the underground pipe network in Wuhou District were imported based on GIS data, comprising 83 nodes and 85 pipes. The average value of the node elevation parameter is approximately 2.89 meters. The length of the pipes ranges from 0.8 to 46.3 meters. In SWMM, the dynamic wave routing option is adopted to solve the full Saint-Venant equations, which allows the simulation to capture backwater effects, flow reversal, and pressurized or surcharged conditions that are critical under extreme rainfall. Pipe diameters and slopes are obtained from the drainage network inventory; for records with missing attributes, standard design diameters are used for completion. Conduit roughness is represented by Manning's coefficient and assigned according to typical material ranges reported in the SWMM manual. Infiltration is modeled using the Horton method, where the decay and drying parameters are selected within the typical ranges recommended by SWMM to ensure physically plausible runoff generation.

For the Chengdu case, model calibration and validation follow common SWMM practice summarized in the previous study [37]. Simulated flooding-prone locations and hydrographs are compared against available historical records to confirm that the model reproduces the observed spatial pattern and magnitude of surcharge or overflow.

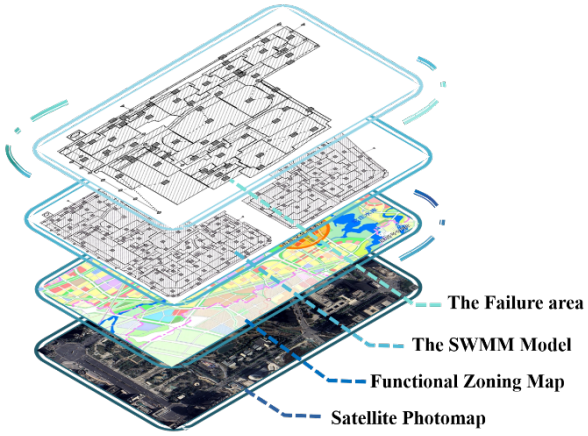

Fig.6. The process of extracting simulation data.

Fig. 6 shows the process of building the SWMM simulation model for the simulation area.

In this study, node statuses and their corresponding failure rates over time are estimated using the MCMC-based simulation process. Node J1, identified as having the highest failure rate, is selected as the initial failure point in the simulation (Fig. 7).

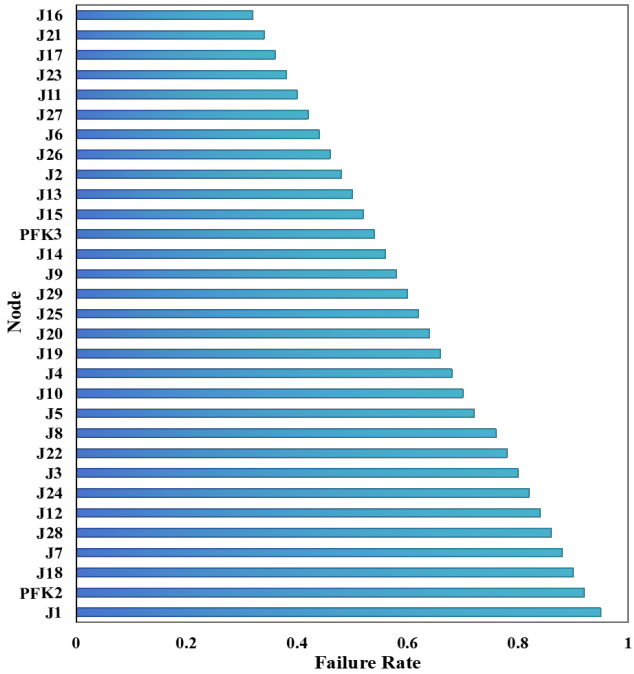

Fig. 7. Node failure rate ranking.

The node with the highest failure rate triggers cascading failures in its adjacent nodes when subjected to prolonged storm impact. Through the MCMC process, the node-state sojourn time is modeled by a Weibull distribution with its shape denoted by k and its scale parameter denoted λ, both of which are estimated by fitting the distribution with from the SWMM-derived sojourn times (node-specific). In this case study, the estimated values $\hat{k} \in [1.5, 3.5]$ and $\hat{\lambda} \in [3, 8]$, where $k$controls the non-constant transition tendency and λcontrols the average state duration (in time units). We can obtain the time and state of cascading failures of the surrounding nodes caused by the J1 failure. Their state change timeline diagrams are shown in Fig. 8.

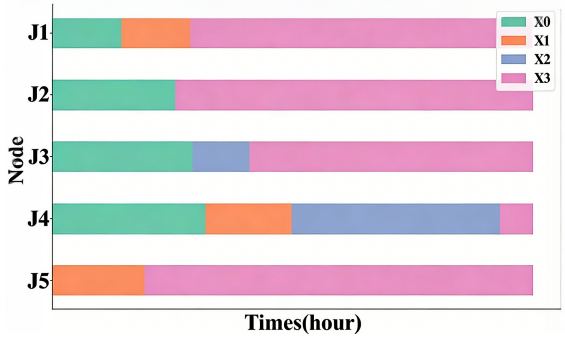

Fig. 8. Timeline diagram of node state changes (J1-J5).

The simulation optimization is carried out in the subsequent simulation based on the cascade failure of nodes from J1 to J5.Combined with the simulation model established on the SWMM simulation platform based on the terrain of a community in Wuhou District and the actual rainfall data from July 11th to 12th, and the cascading failure process obtained from MCMC calculation, the operation status of the underground water pipe network system in this area during the rainstorm from July 11th to 12th, 2023 was simulated. The specific model state conceptual diagram with cascading failure nodes is shown in Fig. 9.

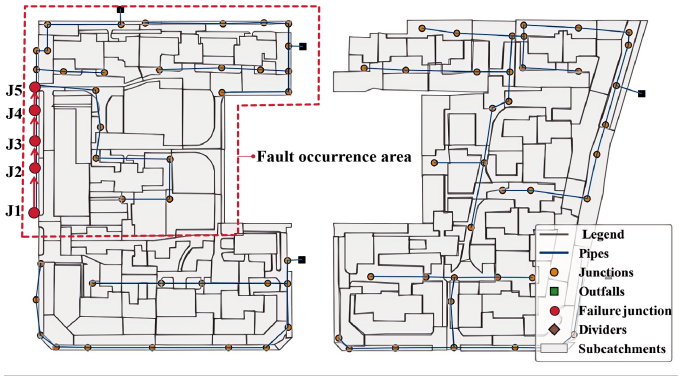

Fig. 9. Diagram of the model's initial state.

NSGA-II is used to determine the optimal node repair sequence and is compared with alternative strategies under the same SWMM-based simulation settings. An initial population of 50 candidate repair sequences (permutations of the repair nodes, e.g., J1–J5) is randomly generated, and the evolution runs for 50 generations. Each generation applies non-dominated sorting and crowding-distance based selection, order-based crossover, and swap mutation (mutation rate=0.2).

During the fitness evaluation phase, the model experienced a cascade failure at 1:00 on July 11th, and different repair strategies were implemented from 2:00 onward for comparative analysis. An external script is used to extract node-level information, including water depth, flow, and capacity. The cost and resilience of each candidate maintenance strategy are calculated by integrating the outputs of the SWMM simulation. To reflect both the intrinsic importance of a node and the practical difficulty of intervention, we express the total cost as the sum of the base repair costs per node:

$$C_{total,i} = 1000\frac{Q_{max,i}}{Q_{max}} + 500\frac{H_{max,i}}{H_{max}} + 300\frac{E_i}{E_{max}}, \quad (26)$$

where $Q_{max,i}$ and $H_{max,i}$ denote the node's maximum flow and maximum water depth, respectively, and E_i is the number of directly connected links (degree). All three attributes are normalized by fixed network-wide reference maxima (Q_{max}, H_{max}, E_{max}) taken from the baseline configuration to ensure cross-strategy comparability. The coefficients represent normalized unit-cost weights for major intervention types. Their relative magnitudes follow Chengdu's municipal cost structures. During implementation, these coefficients can be anchored to local construction cost bulletins or engineering quota manuals.

While $C_{total,i}$ captures node importance, a sequence-sensitive adjustment is introduced so that the total cost depends on when each node is repaired within a strategy. Let $\mathcal{S}$ denote a strategy of candidate failure nodes' repair sequence and t_k the start time at which the k-th repaired node i_k in strategy $\mathcal{S}$ is intervened (determined from the SWMM-driven timeline). The sequence-sensitive total cost of strategy $\mathcal{S}$ is calculated as:

$$C_{total}(\mathcal{S}) = \sum_{k=1}^{m} C_{total,i_k} f(i_k, t_k), \quad (27)$$

$$f(i_k, t_k) = 1 + \alpha\frac{H_{i_k}(t_k)}{H_{i_k,max}} + \gamma, \quad (28)$$

$$\gamma = \begin{cases} 1, & t_k \in [22{:}00, 06{:}00] \\ 0, & \text{Others} \end{cases}. \quad (29)$$

Here H_{i_k} is the simulated water depth of node i_k at its repair's start time t_k, $H_{i_k,max}$ is the maximum permissible water depth of that node. The environmental parameter α and the night-time premium parameter γ can be scenario-tuned (e.g., $\alpha \in [0.2,0.8]$, $\gamma \in [0.1,0.2]$).

This sequence-sensitive formulation operationalizes the 'Cascade-aware control' mechanism (Mechanism 3) of the R^4-UDN architecture. By penalizing delayed interventions $f(i_k, t_k)$ based on real-time water levels, the objective function forces the optimizer to prioritize nodes that—if left unrepaired—would trigger widespread cascading failures, thereby aligning economic costs with systemic risk mitigation. Even with identical repair node sets, different orders alter t_k and thus $H_{i_k}(t_k)$ and the day/night condition, enabling the cost objective to contribute meaningfully to the NSGA-II Pareto optimization.

The performance values at each moment are then calculated from this data. The resilience assessment is divided into three phases: resistance resilience, absorption resilience, and recovery resilience. These phases are measured and combined to produce the overall resilience index using the integral area method of the performance curves.

Non-dominated sorting ranks the population, and then the diversity of the solution set is maintained by calculating the crowding distance for each individual. A tournament selection method chooses parents from the high-quality individuals, followed by permutation crossover and mutation to produce offspring. The population is evaluated through simulation, and then non-dominated sorting and crowding distance calculation are performed again to create the next generation. The process ends after 50 cycles.

C. Results and Discussion

Under the specified simulation parameter settings, this study uses the NSGA-II algorithm to identify the optimal node repair sequence through an evolutionary process over 50 generations. The best repair strategy is compared with alternative approaches by inputting them into the simulation software, with a focus on the multidimensional performance of the urban underground drainage network under different strategies. The results show that the optimal repair strategy identified in this study has significant advantages.

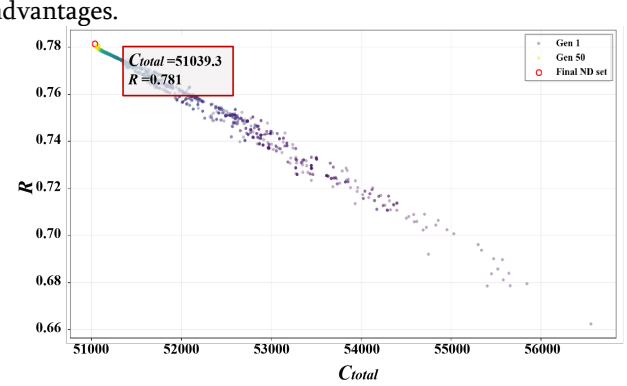

Fig. 10. NSGA-II Pareto front evolution for the two-objective optimization problem.

Fig. 10 illustrates the evolution of the Pareto front throughout the optimization process for two objectives: total cost C_{total} and resilience R. Solutions from the first generation are widely dispersed, while later generations converge toward a narrow, well-defined Pareto front. The final non-dominated set (highlighted in red) includes the optimal solution with $C_{total} = 51039.3$ and $R = 0.781$. This convergence pattern demonstrates the algorithm's effectiveness in navigating the search space and achieving a balanced optimization outcome.

The original system without any human intervention, as well as two strategies with the same repair time and number of nodes but different repair sequences, are selected for comparison in this paper. Fig. 11 compares the multidimensional performance of the urban underground drainage network across different strategies, including the baseline scenario without intervention (Original) and three alternative repair sequences. The superior performance of Strategy 1 (J2 → J1 → J3 → J5 → J4) during the initial rainfall phase validates the effectiveness of the cascade-aware control. Unlike Strategy 2 (J4 → J5 → J3 → J1 → J2) and Strategy 3 (J5 → J4 → J3 → J2 → J1), which treats nodes equally, Strategy 1 identifies and repairs the cascade-initiating nodes (J1–J5) early.

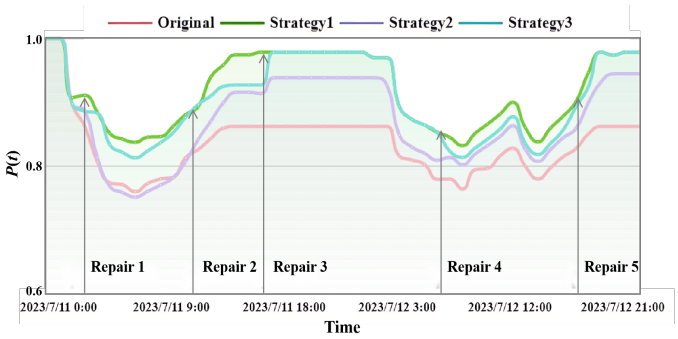

Fig. 11. Comparative system performance under different repair strategies during cascading failure events.

The original system, without intervention, exhibits a sharp decline in performance during the storm, reaching a minimum value of 0.760, indicating limited resistance to extreme rainfall events. Strategy 1 shows a clear performance advantage in the initial rainfall phase, with a minimum performance of 0.832, which is significantly higher than that of the other strategies. During the critical phase (early morning of July 12th) when the rainfall intensity peaked (120 mm/h), the performance of Strategy 1 remained at a high level, reflecting the strategy's reasonable arrangement of node maintenance sequence. The overall performance of Strategies 2 and 3 was between that of the original system and Strategy 1, but at the peak of the rainfall. Both perform less well than Strategy 1.

To enable a consistent cross-strategy comparison, all resilience indicators are standardized by setting the original scenario's minimum performance (0.760) as the baseline for integration, thereby ensuring comparability across resistance, absorption, and recovery phases.

Specific calculation results are presented in Fig. 12. The color-coded regions indicate the integral areas between the performance curve $P(t)$ and the minimum performance baseline across different resilience stages (resistance, absorption, and recovery). Without any intervention, the system exhibits the lowest resistance resilience (0.760), along with insufficient absorption (0.371) and recovery resilience (0.500), resulting in a limited overall resilience score of 0.6042. The comprehensive resilience index is only 0.6042, indicating that the urban underground drainage network's performance in the face of heavy rainfall events without intervention is relatively poor.

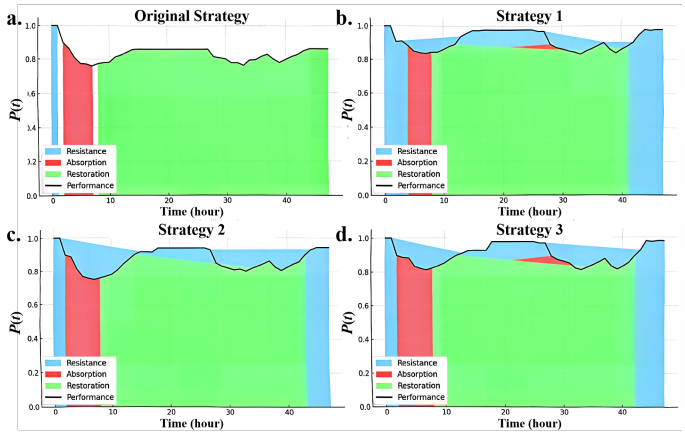

Fig. 12. Map of multi-stage resilience indicators across different strategies.

Strategy 1 demonstrates superior performance across all three resilience phases, with particularly notable improvements in recovery (0.761), leading to the highest comprehensive resilience index of 0.7819. Strategy 3 has the next highest comprehensive resilience (0.7396) and maintains a higher level in the absorption phase (0.677), but it has a slightly lower recovery ability than Strategy 1. Strategy 2 exhibits relatively weak performance in the absorption phase (0.405) but shows a steady increase in performance in the recovery phase, resulting in a comprehensive resilience index of 0.6127.

This comprehensive resilience gain (0.7819) attests to the efficacy of the R⁴-UDN's resimulation-in-loop mechanism. By dynamically evaluating the hydraulic feedback of each repair action, the framework successfully identified a solution that balances immediate resistance with long-term recovery, a trade-off that static optimization methods failed to capture."

VI. Conclusions

Enhancing the resilience of underground drainage systems under extreme rainfall requires more than just incremental improvements to existing IoT frameworks. In this study, we aimed to go beyond the traditional four-layer structure and designed a resilience-focused architecture—R⁴-UDN (Resilience-Ready, Risk-Aware, Resimulation-in-loop, Redundant for Underground Drainage Networks)—that integrates resilience as a core design principle rather than a secondary evaluation step. What sets R⁴-UDN apart is not merely the re-labelling of layers, but the introduction of four interconnected mechanisms that transform sensing, communication, control, and evaluation into a single, closed-loop system.

Our findings demonstrate that R⁴-UDN enhances system responsiveness and data reliability by reconfiguring monitoring intensity through event-triggered sensing. Unlike traditional isolated paradigms, the fusion of resimulation-in-loop and cascade-aware control integrates physical feasibility with systemic risk propagation. By embedding a multi-stage resilience index into a semi-Markov-SWMM model, the framework captures both temporal complexity and hydraulic realism in cascading failures. Furthermore, optimization using sequence-sensitive costs and NSGA-II yields actionable trade-offs between resilience and expenditure. The Chengdu case study confirms that Strategy 1 achieves superior resistance, absorption, and recovery, proving that correctly aligned system-level mechanisms can significantly enhance resilience without necessitating disproportionate costs.

Future studies will further improve the deployment of the R⁴-DUN architecture in practical models. Specifically, upcoming research should incorporate IoT-specific performance constraints—such as signal attenuation, data packet loss, and sensing reliability—into the resilience optimization model to account for the inherent uncertainties of underground communication. Furthermore, we intend to mathematically formalize the event-triggered sensing mechanism, optimize the trade-offs between energy-efficient monitoring and the sensitivity of anomaly detection during extreme events. Transitioning from post-disaster repair sequence optimization to real-time active hydraulic regulation (e.g., adaptive pump and gate control) would further enhance the system's dynamic responsiveness. Additionally, extending this framework to interdependent infrastructures and embedding stakeholder perspectives into cross-layer KPI alignment will bridge the technical-social divide and strengthen the practical relevance of urban resilience planning.

Finally, future studies will broaden the scope by investigating multiple rainfall scenarios, larger networks, and a wider range of system conditions. While the current model has proven effective for the demonstration case in Chengdu, incorporating various rainfall intensities and geographical variations will improve the robustness of the conclusions. Simulations under diverse conditions will provide a more comprehensive understanding of the system's performance and resilience, enhancing the generalizability of the model to different urban contexts and helping to refine strategies for optimizing resilience across a variety of scenarios.

In summary, this work demonstrates that rethinking architecture, through mechanisms such as R⁴-UDN, can open up new avenues for modeling, measuring, and enhancing resilience. Although challenges remain, the results indicate that resilience is not just a performance outcome but also a design principle that, when clarified, can guide both theory and practice in creating future sponge cities.

References

[1] H. Ren, B. Pang, G. Zhao, H. Yu, P. Tian, and C. Xie, "Incorporating dynamic drainage supervision into deep learning for accurate real-time flood simulation in urban areas," *Water Res.*, vol. 270, p. 122816, Feb. 2025, DOI: 10.1016/j.watres.2024.122816.

[2] Y. Yang, H. Guo, D. Wang, X. Ke, S. Li, and S. Huang, "Flood vulnerability and resilience assessment in China based on super-efficiency DEA and SBM-DEA methods," *J. Hydrol.*, vol. 600, p. 126470, Sept. 2021, DOI: 10.1016/j.jhydrol.2021.126470.

[3] A. C. R. Lopes, O. M. Rezende, and M. G. Miguez, "Urban resilience to floods in the context of the disaster risk management cycle: a literature review," *J. Hydrol.*, vol. 662, p. 133827, Dec. 2025, DOI: 10.1016/j.jhydrol.2025.133827.

[4] J. L. Webber, T. Fletcher, R. Farmani, D. Butler, and P. Melville-Shreeve, "Moving to a future of smart stormwater management: A review and framework for terminology, research, and future perspectives," *Water Res.*, vol. 218, p. 118409, June 2022, DOI: 10.1016/j.watres.2022.118409.

[5] A. Salam and S. Shah, "Urban Underground Infrastructure Monitoring IoT: The Path Loss Analysis," *in Proc. IEEE 5th World Forum on Internet of Things (WF-IoT)*, Limerick, Ireland: IEEE, Apr. 2019, pp. 398–401. DOI: 10.1109/WF-IoT.2019.8767358.

[6] P. Pătraşcu and G.-F. Nicoară, "Adopting IoT Solutions for the Functionality, Protection and Resilience of Critical Infrastructures," *in Proc. 17th Int. Conf. Eng. Mod. Electr. Syst. (EMES)*, June 2023, pp. 1–6. DOI: 10.1109/EMES58375.2023.10171624.

[7] Ayush, P. Singh, P. Jain, V. Saini, K. Kumari, and P. Kumar Bajaj, "Enhancing Smart City Infrastructure Through IoT-Enabled Predictive Maintenance and Real-Time Data Analytics," *in Proc. 2024 Int. Conf. Prog. Innov. Intell. Syst. Data Sci. (ICPIDS)*, Dec. 2024, pp. 129–137. DOI: 10.1109/ICPIDS65698.2024.00029.

[8] E. H. Houssein, M. A. Othman, W. M. Mohamed, and M. Younan, "Internet of Things in Smart Cities: Comprehensive Review, Open Issues, and Challenges," *IEEE Internet Things J.*, vol. 11, no. 21, pp. 34941–34952, Nov. 2024, DOI: 10.1109/JIOT.2024.3449753.

[9] J. Liang, H. Zhang, X. Deng, and Z. He, "On Zone-Differentiated Time-Constrained Flow Capacity Intelligent Monitoring for Large-Scale Urban Pipeline Systems by Mobile Sensors," *IEEE Internet Things J.*, vol. 9, no. 23, pp. 23599–23613, Dec. 2022, DOI: 10.1109/JIOT.2022.3151345.

[10] B. Liu, Q. Feng, L. Zhong, and Y. Chen, "Physical-Information-Functional Architecture for Internet of Things," *IEEE Internet Things J.*, pp. 1–1, 2025, DOI: 10.1109/JIOT.2025.3593339.

[11] H. Dui, H. Zhang, and S. Wu, "A IoT-based novel methodology to optimize multidimensional flood resilience of drainage systems for sponge city," *Sustain. Cities Soc.*, vol. 130, Art. no. 106523, 2025, DOI: 10.1016/j.scs.2025.106523.

[12] K. Eckart, Z. McPhee, and T. Bolisetti, "Multiobjective optimization of low impact development stormwater controls," *J. Hydrol.*, vol. 562, pp. 564–576, July 2018, DOI: 10.1016/j.jhydrol.2018.04.068.

[13] F. Dong, Z. Zhang, C. Liu, R. Zou, Y. Liu, and H. Guo, "Towards efficient Low Impact Development: A multi-scale simulation-optimization approach for nutrient removal at the urban watershed," *J. Clean. Prod.*, vol. 269, p. 122295, Oct. 2020, DOI: 10.1016/j.jclepro.2020.122295.

[14] M. R. Hassani, S. F. Mousavi Janbehsarayi, M. H. Niksokhan, and A. Sharma, "Intersecting social welfare with resilience to streamline urban flood management," *Sustain. Cities Soc.*, vol. 116, p. 105927, Dec. 2024, DOI: 10.1016/j.scs.2024.105927.

[15] R. He, R. L. K. Tiong, Y. Yuan, and L. Zhang, "Enhancing resilience of urban underground space under floods: Current status and future directions," *Tunn. Undergr. Space Technol.*, vol. 147, p. 105674, May 2024, DOI: 10.1016/j.tust.2024.105674.

[16] B. Cao, Y. Zhang, J. Zhao, X. Liu, L. Skonieczny, and Z. Lv, "Recommendation Based on Large-Scale Many-Objective Optimization for the Intelligent Internet of Things System," *IEEE Internet Things J.*, vol. 9, no. 16, pp. 15030–15038, Aug. 2022, DOI: 10.1109/JIOT.2021.3104661.

[17] Y. Chen, P. Cowling, F. Polack, S. Remde, and P. Mourdjis, "Dynamic optimisation of preventative and corrective maintenance schedules for a large scale urban drainage system," *Eur. J. Oper. Res.*, vol. 257, no. 2, pp. 494–510, Mar. 2017, DOI: 10.1016/j.ejor.2016.07.027.

[18] Q. Zhang, Y. Liu, B. Zhang, and H.-Z. Huang, "Selective Maintenance Optimization Under Limited Maintenance Capacities: A Machine Learning-Enhanced Approximate Dynamic Programming," *IEEE Trans. Rel.*, vol. 74, no. 3, pp. 4320–4334, Sept. 2025, DOI: 10.1109/TR.2024.3459649.

[19] M. Rabbani, R. Heidari, and R. Yazdanparast, "A stochastic multi-period industrial hazardous waste location-routing problem: Integrating NSGA-II and Monte Carlo simulation," *Eur. J. Oper. Res.*, vol. 272, no. 3, pp. 945–961, Feb. 2019, DOI: 10.1016/j.ejor.2018.07.024.

[20] K. Deb, A. Pratap, S. Agarwal, and T. Meyarivan, "A fast and elitist multiobjective genetic algorithm: NSGA-II," *IEEE Trans. Evol. Comput.*, vol. 6, no. 2, pp. 182–197, Apr. 2002, DOI: 10.1109/4235.996017.

[21] B. Doerr and Z. Qu, "A First Runtime Analysis of the NSGA-II on a Multimodal Problem," *IEEE Trans. Evol. Computat.*, vol. 27, no. 5, pp. 1288–1297, Oct. 2023, DOI: 10.1109/TEVC.2023.3250552.

[22] M. Shahed Behrouz, D. J. Sample, and M. Nayeb Yazdi, "Robustness of storm water management model parameter sets for dry and wet hydroclimatic conditions," *J. Clean. Prod.*, vol. 411, p. 137328, July 2023, DOI: 10.1016/j.jclepro.2023.137328.

[23] L. Rosenberger, J. Leandro, and B. Helmreich, "Enhancing SWMM-UrbanEVA for continuous long-term water balance analysis of green infrastructure," *Sustain. Cities Soc.*, vol. 128, p. 106475, June 2025, DOI: 10.1016/j.scs.2025.106475.

[24] S. Wang, J. Wang, K. Xin, H. Yan, S. Li, and T. Tao, "Enhancing real-time urban drainage network modeling through Crossformer algorithm and online continual learning," *Water Res.*, vol. 268, p. 122614, Jan. 2025, DOI: 10.1016/j.watres.2024.122614.

[25] W. Tian, Z. Zhang, K. Xin, Z. Liao, and Z. Yuan, "Enhancing the resilience of urban drainage system using deep reinforcement learning," *Water Res.*, vol. 281, p. 123681, Aug. 2025, DOI: 10.1016/j.watres.2025.123681.

[26] Liu, X., Wu, X., Li, X., Xu, X., Liao, W., Jiao, L., Zeng, Z., Chen, G., Li, X., "Global mapping of three-dimensional urban structures reveals escalating utilization in the vertical dimension and pronounced building space inequality," *Eng.*, vol. 47, pp. 86–99, Apr. 2025, DOI: 10.1016/j.eng.2024.01.025.

[27] B. Zhang, Y. Liu, and Y.-X. Zheng, "Dynamic Reliability Assessment of Hierarchical Multistate Systems With Sensors' Degradation," *IEEE Trans. Rel.*, vol. 74, no. 3, pp. 3784–3798, Sept. 2025, DOI: 10.1109/TR.2024.3524098.

[28] H. Dui, H. Zhang, X. Dong, S. Wu, and Y. Wang, "IoUT-enhanced cooperative control scheme for multiple AUVs with IoT data reliability," *IEEE Trans. Intell. Transp. Syst.*, pp. 1–16, 2025, DOI: 10.1109/TITS.2025.3535737.

[29] H. Dui, H. Zhang, and S. Wu, "Spatiotemporal resilience of IoT-enabled unmanned system of systems," *Eng.*, vol. 32, no. 5, pp. 100–117, 2025, DOI: 10.1016/j.eng.2025.03.012.

[30] K. Wang, Z. Xu, Y. Liu, and Y. Fang, "Resilience Enhancement for Multistate Interdependent Infrastructure Networks: From a Preparedness Perspective," *IEEE Trans. Rel.*, vol. 72, no. 1, pp. 190–203, Mar. 2023, DOI: 10.1109/TR.2021.3132774.

[31] T. Xiahou, Z. Zeng, Y. Liu, and H.-Z. Huang, "Fusing Conflicting Multisource Imprecise Information for Reliability Assessment of Multistate Systems: A Two-Stage Optimization Approach," *IEEE Trans. Rel.*, vol. 72, no. 1, pp. 90–105, Mar. 2023, DOI: 10.1109/TR.2022.3187075.

[32] H. Dui, H. Zhang, X. Dong, and S. Zhang, "Cascading failure and resilience optimization of unmanned vehicle distribution networks in IoT," Reliab. Eng. Syst. Saf., vol. 246, p. 110071, June 2024, DOI: 10.1016/j.ress.2024.110071.

[33] H. Wang, X. Pan, Z. Liu, Y. Dang, and D. Hong, "A Framework for the Network-Based Assessment of System Dynamic Resilience," *IEEE Trans. Rel.*, vol. 74, no. 1, pp. 2448–2458, Mar. 2025, DOI:

10.1109/TR.2024.3371215.

[34] Y. Zheng, X. Jin, J. Wei, Y. Zhou, and Y. Zhang, "A novel framework for optimization and evaluation of sensors network in urban drainage system," *Water Res.*, vol. 270, p. 122833, Feb. 2025, DOI: 10.1016/j.watres.2024.122833.

[35] Q. Zhang, Y. Liu, L. Xing, and H.-Z. Huang, "Reliability Modeling and Assessment of Internet-of-Things in Smart Manufacturing Systems: A Modular Petri Net Approach," *IEEE Trans. Rel.*, pp. 1–15, 2025, DOI: 10.1109/TR.2025.3606866.

[36] L. A. Rossman, *Storm Water Management Model Reference Manual, Volume II: Hydraulics*, EPA/600/R-17/111. Cincinnati, OH, USA: U.S. Environmental Protection Agency, Office of Research and Development, May 2017.

[37] M. Niazi, C. Nietch, M. Maghrebi, N. Jackson, B. R. Bennett, M. Tryby, and A. Massoudieh, "Storm water management model: performance review and gap analysis," *J. Sustainable Water Built Environ.*, vol. 3, no. 2, p. 10.1061/jswbay.0000817, Jan. 2017, doi: 10.1061/jswbay.0000817.

Hongyan Dui received the Ph.D. degree in management science and engineering from Northwestern Polytechnical University, China, in 2013. He visited the systems engineering and engineering management, City University of Hong Kong many times as a research fellow from 2014 to 2019.

He is a Professor with the School of Management, Zhengzhou University, Zhengzhou, China. His recent research interests include the reliability engineering, importance measure theory, deep learning, and risk decision making. He has published over 100 journal articles. He was honored to be within the top 2% Ranking of Scientists in the World by Stanford University.

Ran Li is currently pursuing the Ph.D. degree with the School of Management, Zhengzhou University, Zhengzhou, China.

Her research interests include urban resilience, multi-objective optimization, and the IoT systems and applications.

Huanqi Zhang is currently pursuing the Ph.D. degree with the School of Management, Zhengzhou University, Zhengzhou, China.

His research interests include reliability model, wireless sensor networks, and the IoT systems and applications.

Shaomin Wu received the M.Sc. and Ph.D. degrees in applied statistics. Before moving to the University of Kent, he was a Senior Lecturer in risk and decision analysis at Cranffeld University. His research interests include recurrent event data analysis, machine learning, risk analysis, and security analysis. He is a member of the editorial boards of seven journals.